Available online at www.sciencedirect.com
SCIENCE DIRECT®
Acta Materialia 52 (2004) 1097–1105
Acta MATERIALIA
www.actamat-journals.com

Surface oxide cracking associated with oxidation-induced grain boundary sliding in the underlying alloy

J.A. Nychka, C. Pullen, M.Y. He, D.R. Clarke *

Materials Department, College of Engineering, University of California, Santa Barbara, CA 93160-5050, USA

Received 11 June 2003; received in revised form 27 October 2003; accepted 29 October 2003

Abstract

When thin sections of FeCrAlY alloys having initially flat surfaces are oxidized at high temperature, the surface becomes uneven as some metal grains on the surface displace above and below the macroscopic surface. On subsequent cooling, the oxide formed by high-temperature oxidation cracks and spalls at the edges of the uplifted grains. Microstructural observations indicate that the grain uplift is associated with grain sliding and it proposed that the sliding at the oxidation temperature occurs in response to the evolving compressive growth stress in the oxide. The observed spalling patterns are consistent with a fracture mechanics model in which incipient flaws at the oxide-alloy interface, in the vicinity of the step edges, propagate in the residual stress field in the oxide.

Keywords: Oxidation; Growth stress; Grain boundary sliding; Fracture; Spalling

1. Introduction

During the course of studying the high temperature oxidation of alumina-forming alloys, such as the FeCrAlY alloys, we have noticed a previously unreported form of oxide spalling after cooling the alloys down to room temperature. Two distinct observations have been made. The first is that after oxidation, initially flat and polished alloy surfaces developed an uneven surface with individual metal grains protruding above the surface even though the surface remains macroscopically flat. The second observation is spalling of the oxide on cooling with a preference for its occurrence along the periphery of some of the uplifted grains. These two phenomena are illustrated in the optical micrograph of Fig. 1 and the scanning electron micrograph of Fig. 2. The striking feature of these observations is that they only occurred with relatively thin plates or small diameter wires of the alloys. The observation of oxide spalling was also particularly surprising since the oxide typically does not crack and spall at all when thick samples of the same alloys with clean, smooth surfaces are oxidized. Thin sheets of these alloys are now of interest as catalyst supports and fuel cell electrodes in addition to their traditional use in electrical heating elements.

These unexpected observations motivated a more systematic exploration, described herein, of the responsible mechanisms. The work also extends upon previous experiments [1,2] in which it was shown that thin plates of FeCrAlY alloy elongate during oxidation in response to the development on a compressive stress in the thermally grown oxide as it thickens with continuing oxidation. On the basis of the results of these earlier experiments, together with additional experiments described below, the phenomenon of grain upheaval is found to be associated with grain boundary sliding in the alloy as it plastically deforms to relax the lateral growth stress in the oxide accompanying oxidation. A simple fracture mechanics model is introduced to describe the conditions for the fracture and spalling of the oxide from the edge of an uplifted grain on cooling.

* Corresponding author. Tel.: +1-8058938275; fax: +1-8058938983.
E-mail address: clarke@engineering.ucsb.edu (D.R. Clarke).

1359-6454/$30.00 © 2003 Acta Materialia Inc. Published by Elsevier Ltd. All rights reserved.
doi:10.1016/j.actamat.2003.10.042

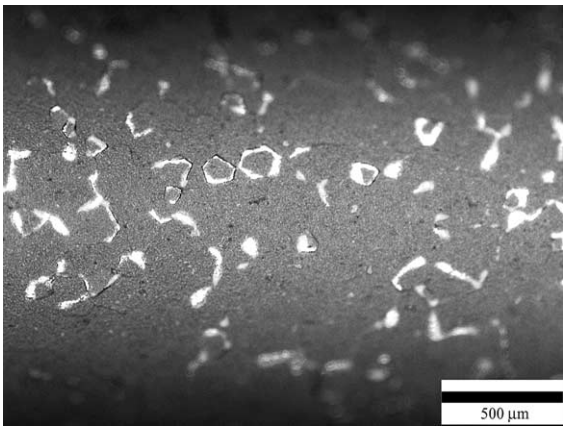

Fig. 1. Low magnification, reflected light micrograph revealing the presence of bare metal around the periphery of the alloy grains where the oxide had spalled away. Under the imaging conditions used, the metal is highly reflective and hence appears much brighter than the oxide covered regions. Wire oxidized isothermally for 10 h at 1200 °C.

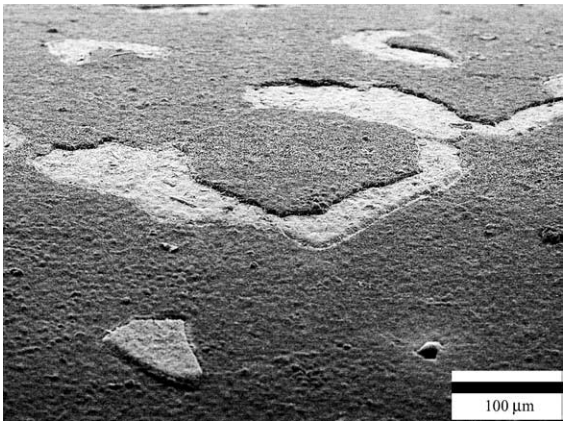

Fig. 2. Higher magnification view of the spallation failure of the oxide along grain boundaries in the underlying alloy.

2. Experiments and observations

Oxidations experiments were performed on thin plates and small diameter wires of three different FeCrAlY alloys. The experiments on the wires were carried out to determine the extent of plastic elongation on oxidation and its dependence on diameter to complement the quantitative measurements of the thickness dependence of the plastic strain previously obtained with the plates [1]. Two different thin alloy plates were investigated, a solution hardened Fe-22a/oCr-5.8a/oAlY alloy (from Goodfellow Metals) and a commercially available, dispersion-strengthened MA 956 alloy. (The latter is mechanically alloyed, contains Y_2O_3 particles and has a nominal composition of Fe-20a/oCr-5a/oAl). The wires were of a Kanthal A1 alloy, an alloy of a slightly different composition (Fe-21.2a/oCr-5.6a/oAlY) than the FeCrAlY plates. Prior to oxidation, all the alloys were first annealed in vacuum at 1100 °C for 20 h to promote recrystallization and to stabilize the grain structure of the alloys. The surface oxide was then removed by superficial grinding and the surfaces polished using 3 μm diamond paste and solvent cleaned prior to subsequent oxidation. Prior to oxidation, a deep groove was made several centimeters from both ends of each wire to serve as a fiducial mark. (The off-set distance was based on the results of preliminary experiments, using photostimulated luminescence [3], of the residual stress in the oxide versus distance from the end. The fiducial mark was made further from the ends than the characteristic stress transfer length). The distance between the fiducial marks was measured using a high-precision traveling optical micrometer.

Short lengths of wires, whose diameters ranged from 5 mm down to 200 μm, were oxidized in air for different times and temperatures. After oxidizing, they were either cooled rapidly by pulling out of the furnace or slowly cooled (~8 K/min) by leaving them in the furnace and the furnace turned off. Full details of the oxidation results, including measurements of the stress in the oxide, oxidation kinetics and temperature dependence are to be described elsewhere. However, pertinent to this work are the results of plastic elongation produced by oxidation. These results, obtained after oxidation at 1200 °C, are shown in Fig. 3 for both the rapid and slowly cooled wires. As the accuracy of the plastic strain measurements is estimated to be ±0.1%, these data indicate that there is little or no plastic elongation for wire diameters greater than 2 mm but a strong dependence on diameter for smaller wire diameters. The greater elongation on slow cooling than on fast cooling is attributed to continued plastic deformation during cooling. The cooling rate dependence is consistent with earlier measurements on sheet samples of different thickness' that indicated that stress relaxation in the oxide occurs by plastic deformation of the FeCrAlY

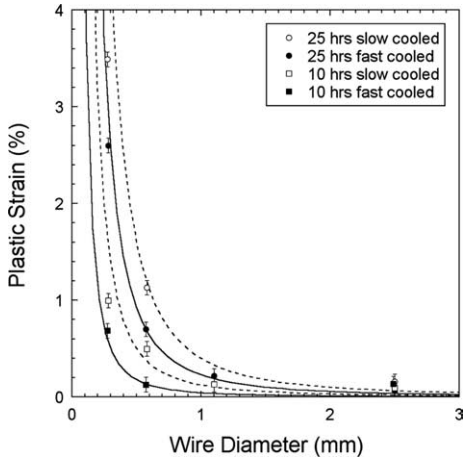

Fig. 3. Plastic elongation of FeCrAlY wires of different diameters after oxidation at 1200 °C. The lines are guides to the eye.

alloy down to a temperature of ~800 °C [4]. Observations of the wire surfaces revealed only occasional oxide spalling on the 2.59 mm wires with more extensive spalling on the smaller diameter wires.

To characterize the oxidation-induced grain upheaval, the top and bottom surfaces of the plates were examined before and after oxidation under oblique lighting. An example of the evolution of grain upheaval is shown in Fig. 4 of the surface of a polished, initially 872 μm thick Fe-22a/oCr-5.8a/oAlY plate after oxidizing different parts of the plate in air at 1200 °C for 27, 51 and 315 h and then slow cooling. The oblique lighting reveals an uneven surface associated with individual grains and an increase in the magnitude of the surface upheaval with oxidation time. No such contrast was visible before oxidation. The oblique lighting, from the top right of the image in this particular case, also highlights (by the light or dark contrast from the grain edges) that some grains protrude above the surface, others have moved down and others appear to be undisplaced with respect to their neighbors. Interestingly, no surface upheaval was noted on the dispersion hardened (MA956) alloy after comparable oxidation.

Complementary measurements were made of the plastic extension of the plates and of the residual stress in the oxide using photostimulated luminescence piezospectroscopy [3]. These measurements indicated, for instance, that for the sheet in Fig. 4, the biaxial stress in the oxide steadily decreased from 4.88 to 3.72 GPa as the oxide grew reducing the remaining alloy cross-section. These values are consistent with previous measurements on the same alloy and indicating that there was a stress in the growing oxide of ~1.0 GPa over this period of oxidation [1]. To supplement these quantitative observations, the plates were also cross-sectioned in a number of places. After polishing, the cross-sections were etched in a 1:1:1 mixture of nitric acid, hydrochloric acid and water to reveal the grain boundaries in the alloy. The cross-sections revealed that some of the grains had slid relative to their neighbors as shown in Fig. 5(a). No sliding was observed, however, when the grain boundaries were perpendicular to the surface as shown in Fig. 5(b). The relative vertical displacement of sliding grains varied substantially from boundary to boundary, as indicated in Fig. 4, as well as being dependent on the grain boundary angle as shown in Fig. 5. Significantly, the cross-section also reveals that the oxide is continuous along the surface of the grains and their edges, suggesting that the grains were sliding during oxidation rather than on cooling in response to the thermal expansion mismatch generated stresses on cooling.

Observations of the oxide spalling at high magnifications reveals that the oxide failure occurred principally along the oxide/alloy interface at the step edges of

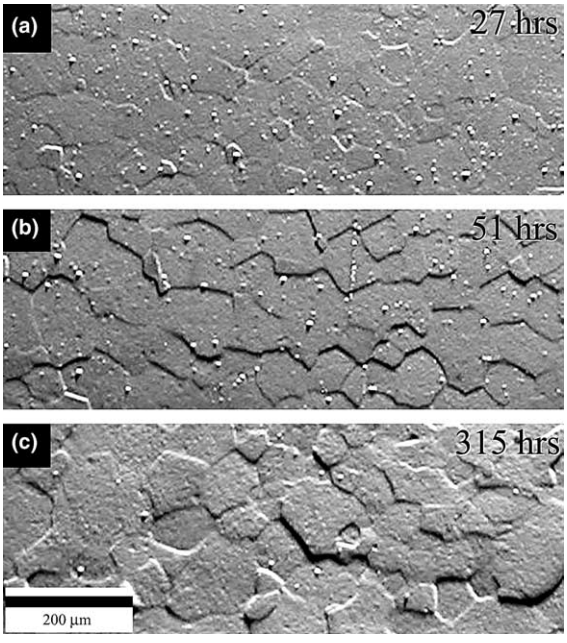

Fig. 4. Evolution in surface relief on parts of an initially flat, polished Kanthal A1 alloy plate after oxidation in air at 1200 °C for 27 h (a), 51 h (b) and 315 h (c) revealed under oblique lighting. After these oxidation times, the sheet had extended by 0.17%, 0.32% and 1.2%, respectively. Optical micrograph.

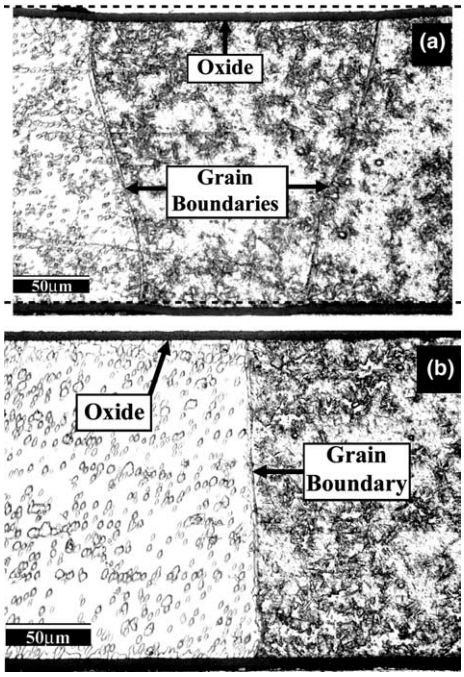

Fig. 5. Cross-sections of an oxidized FeCrAlY alloy exhibiting surface relief after etching. (a) Grain sliding and surface offset where the grain boundaries are inclined to the surface and (b) where the grain boundary is normal to the surface. The oxide has the uniform dark gray appearance and the mottled contrast within the grains is a consequence of the etching used to highlight the grain boundaries. (The horizontal dotted lines are guides to the eye.)

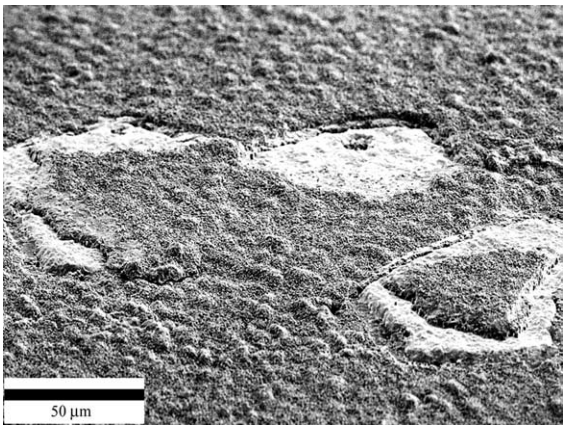

Fig. 6. High magnification SEM image illustrating that oxide spalling has occurred on both the side and top of the corners of three uplifted grains. The exposed metal appears bright.

uplifted grains, as illustrated in Fig. 2. In some cases, the oxide spalled right across the uplifted grains. In other instances, the oxide failed by cracking at the step edges and then, at some distance from the grain edge, the interface crack kinked up from the interface to fracture through the oxide itself and cause the oxide to spall away from the alloy. In either case, the oxide spalls from both the top surface and the side of the step produced by grain uplift. This is illustrated in Fig. 6.

3. Mechanism of grain uplift

The fact that grain uplift and grain sliding upon oxidation were only observed to occur when the alloys were in the form of thin plates or wires suggests that they are a response of the alloy to the compressive stress generated in the oxide as it grows. For FeCrAlY alloys, the compressive growth stress can be as large as 1.5 GPa for oxidation temperatures of 1000–1300 °C [1,2]. This stress, sometimes referred to as the lateral growth stress, develops as a consequence of the formation of the oxide and following Rhines and Wolf [5] is attributed to the formation of new oxide along grain boundaries in the oxide [6]. In order to maintain mechanical equilibrium during oxidation, the compressive stress in the growing oxide must be balanced by a tensile stress in the alloy. This force balance requires, for the flat sheets, that

$$\sigma_m h_m + 2\sigma_G h = 0, \quad (1)$$

where the growth stress in the oxide is denoted as σ_G, the stress in the metal alloy is σ_m and h and h_m are the thickness of the oxide and alloy, respectively. The balance of stresses is shown schematically in Fig. 7 for a uniform thickness oxide formed on a uniform thickness alloy plate. If the tensile stress in the alloy exceeds the appropriate flow stress (creep stress or the plastic yield stress) of the alloy at the oxidation temperature, the alloy will elongate in response to this stress. The rate at which the elongation occurs will, of course, be governed by the constitutive behavior of the alloy but if the plastic deformation of the alloy is homogeneous it will elongate and reduce in section uniformly with no surface displacements. However, the microstructural evidence from micrographs such as Figs. 4 and 5 is that the plastic deformation is accommodated, at least in part, by grain boundary sliding rather than wholly by dislocation plasticity within the grains. The consequence of grain boundary sliding is that grains will displace relative to one another with surface upheavals correlated to the grain size, as shown schematically in Fig. 7.

Eq. (1) indicates that the plastic deformation is dependent on the ratio of the oxide thickness to that of the alloy. This, in turn, supports the notion that grain sliding and grain uplift can only be expected to occur on relatively thin alloy sections, as is observed. The lack of experimental data on the high temperature properties of these alloys precludes a quantitative analysis but according to the manufacturer's limited data for the Kanthal FeCrAlY alloy the creep strength at 1000 °C is ~1 MPa and the short-term tensile strength at 900 °C is 34 MPa [7]. Both can be expected to be substantially smaller at 1200 °C, the temperature at which our oxidation experiments were performed. Nevertheless, an estimate of the tensile stress in the sheet sample shown in Fig. 4 can be obtained by applying Eq. (1). After 27 h oxidation, the oxide was 5.1 μm thick and the sheet thickness had been reduced to 860 μm. Assuming that the growth stress over the time of oxidation was 1 GPa, a reasonable value considering that the measured residual stress at room temperature after the 27 h oxidation was 4.88 GPa, then the tensile stress in the sheet would be ~10 MPa. That this estimate is above the stress at which deformation can be expected is consistent with our measurement that the sheet had extended by a strain of 0.17%.

4. Mechanics model of edge cracking

As already remarked, the nature of the oxide spalling, around the periphery of the uplifted grains, is distinctly different from the typical spalling failure seen following thin-film buckling on flat surfaces. Spalling rarely occurs on any of these FeCrAlY alloys but when it does it takes the form of circular blisters about 100 μm diameter where the oxide "pop-off" on cooling. (Micrographs illustrating these spalls and their temporal evolution have been presented in [8,9]). This circular spall geometry has been the subject of several previous analyzes [10]. In these analyzes a film under biaxial compression, buckles and spalls from a pre-existing flaw at the interface between the film and a semi-infinite substrate, when the flaw is remote from edge of the film. Analysis of the

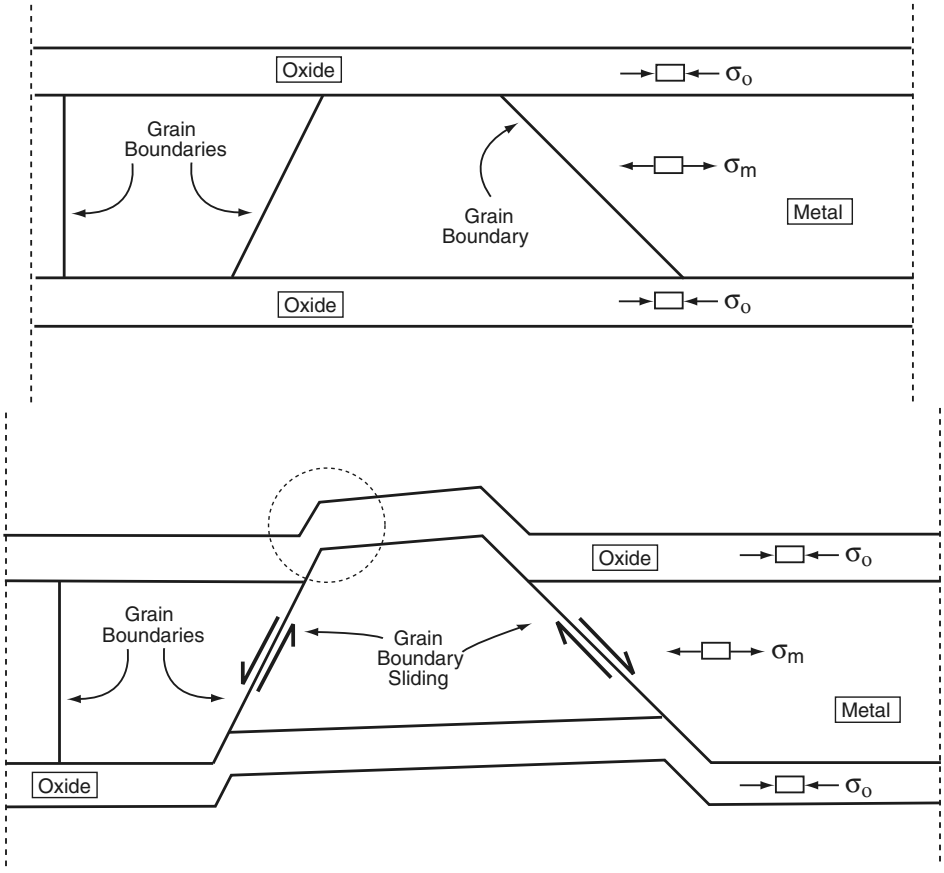

Fig. 7. Schematic diagram illustrating the mechanism of grain uplift when grain boundary sliding occurs to accommodate the plastic extension produced in relaxing the compressive growth stress in the surface oxide as it grows.

cracking when an interface flaw is situated along the edge of a residually compressed film has also been presented [11]. Failure of a compressed film that covers both the side and top of a step has not, to our knowledge, been analyzed so in this section we consider crack propagation at the oxide/alloy interface in the vicinity of a right-angle step as shown schematically in Fig. 8(a). The residual stress, σ_0, is taken to be the sum of the growth stress plus the thermoelastic stress arising from the difference in thermal expansion coefficient on cooling. Well away from the step, the oxide film is under biaxial compression but in the immediate vicinity of the step the residual stress state is not biaxial because the edges themselves must be traction-free. Some insight into the residual stress field can be gained by recognizing that formally a distribution of imaginary forces, P, must be applied to surface of the compressed oxide surfaces at the edge itself in order to render those surfaces traction free. The effect of these forces can be calculated from the distribution of line forces necessary to render the edges traction-free. The latter can be obtained from the Boussinesq stress function, ϕ, for the stress field in a homogeneous infinite body created by a uniformly distributed load having an intensity, P, applied over a plate thickness, h [12]. The principal results of the analysis are that there is a tensile hydrostatic stress field at the corner O, and both a tensile and shear stress along both interfaces that monotonically decreases with distance from the corner. Consequently, a flaw located along the oxide/alloy interface near the edge is subject to mixed-mode loading that changes as the flaw extends. Furthermore, the symmetry of the line forces, P, acting along the oxide also suggests that they would act to create a bending moment on a flaw extending away from a square corner.

To quantify the redistribution of residual stress and the strain energy release rates for flaws at a right-angled step edge, we have performed a series of generalized plane strain, finite element computations using the ABAQUS code. Three flaw configurations at the oxide/alloy interface were considered, as shown schematically in Fig. 8. The first is a slit-shaped crack lying along the top interface at some distance from the edge with one end, A, at a distance, b, from the step in the alloy and the other end, B, is at a distance, a. The second is an edge crack, C, in the oxide in the same plane as the top oxide/alloy interface (Fig. 8(c)). The third is a flaw on both sides of the step-edge, Fig. 8(d). A fine, focused

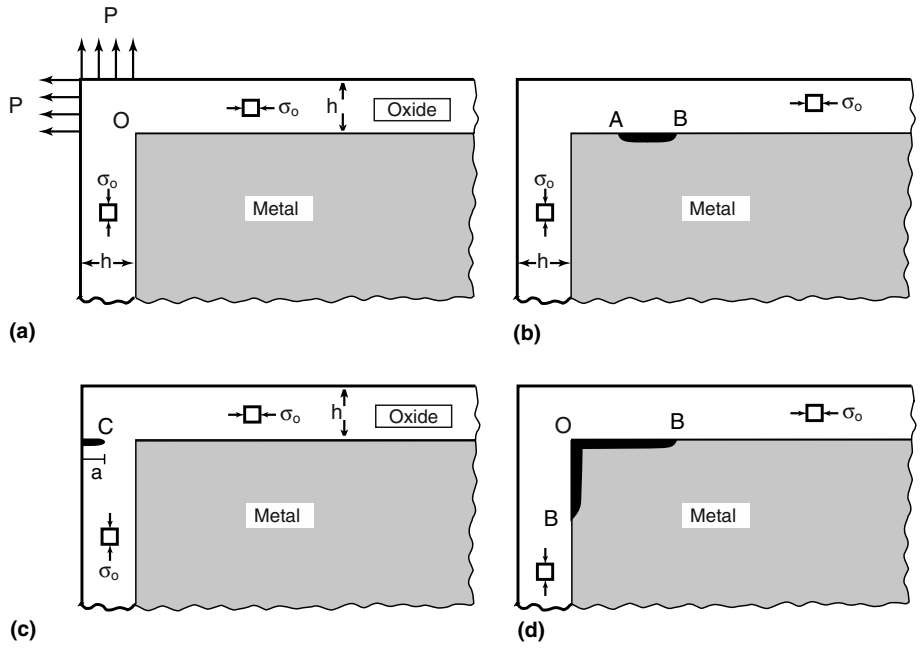

Fig. 8. (a) Schematic diagram illustrating the forces, P, needed to ensure a traction free surface in the vicinity of the corner when the oxide is under compression. In evaluating the strain energy release rates for the propagation of incipient corner flaws, three types of interface flaw are considered: a flaw on the top interface (b), an edge flaw (c) and a flaw on both sides of the corner (d).

mesh with quarter-point crack tip elements was used to model the behavior near the singularity. A convergence study revealed that the meshes used provided accurate values for both the strain energy release rate, G, and stress intensity factor, K. Details of the numerical procedures have been described elsewhere [11,13–15]. The mode I and mode II stress intensity factors, K_{I} and K_{II}, respectively, were obtained from the crack opening displacements as discussed previously [10,14] and the mode mixity calculated. In each case, the calculated strain energy release rates were compared with that for a crack growing asymptotically along the interface of a biaxially compressed film attached to a semi-infinite substrate [10]:

$$G_{\mathrm{SS}} = \frac{(1-\nu_0^2)\sigma_0^2 h}{2E_0}. \tag{2}$$

In the majority of the computations, the elastic moduli of the oxide and alloy were assumed to be the same. For comparison, in a number of calculations the oxide and alloy were given elastic moduli of 400 and 200 GPa, corresponding to those of aluminum oxide and a typical iron based alloy, respectively. The Dundurs parameter, β, used in the computations was zero. Usually, the β parameter plays a secondary role in problems such as those considered here. The details of singularities associated with interfacial cracks are beyond the scope of this paper but can be found elsewhere [10,13,14].

The mixed mode character of crack extension in the vicinity of the step edge is illustrated in Fig. 9 for the propagation of the end B of a flaw with its other end A

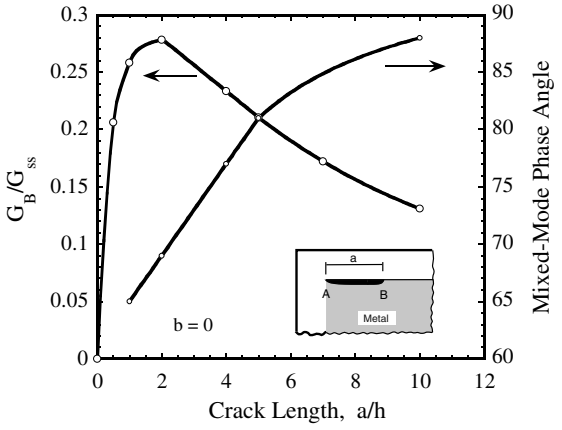

Fig. 9. Strain energy release rates for the end B of the interface crack in the vicinity of the corner with the other end fixed at the corner and computed mixed mode phase angle. Both the oxide film and the alloy have the same elastic constants.

fixed at the step corner. The strain energy release rate rises rapidly as the flaw extends away from the corner, peaks and then slowly decreases with distance. As the crack extends the mixed mode phase angle slowly increases approaching 90° (a mode II condition) after a normalized distance of $a/h = 12$. The more general situation in which the end A is not fixed and lies either along the alloy/oxide interface or extends into the oxide to the side is shown in the computed strain energy release rates of Fig. 10(a) for two different values of a/h. (The divergence in the strain energy release curves at the

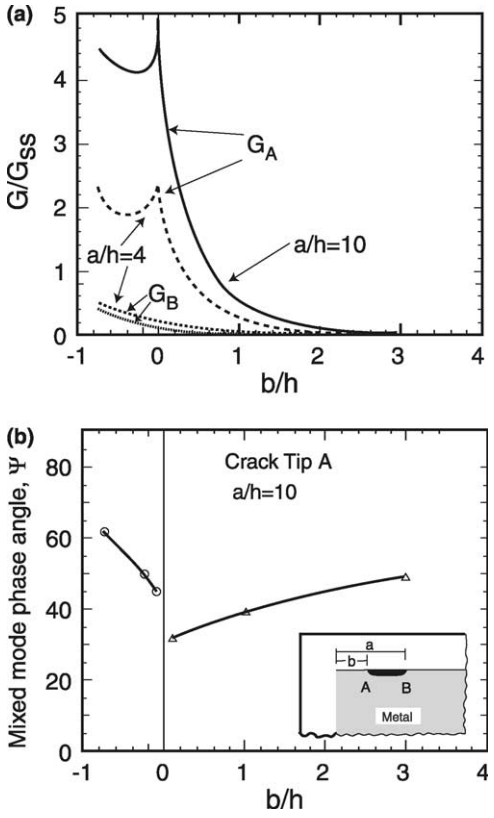

Fig. 10. (a) Strain energy release rate for both ends of the interface crack computed for two crack lengths, a/h. The lowest curve is G_B for a crack length, $a/h = 10$. Negative values for the value of b correspond to the crack extending into the side oxide. (b) Mode mixity at the end A of a crack of $a/h = 10$. Equal elastic constants for the oxide and alloy.

alloy corner, $b/h = 0$, is presumably due to the singularity in the stress fields at the corner, O. The meshes used in these calculations may not give very accurate values for G_A when the ratio b/h approaches zero due to the corner singularity but as the precise values are not of great importance for this work no attempt was made to obtain a precise value). The corresponding phase angle for the crack end A when the other end, B, is fixed at a distance $10h$ from the corner is shown in Fig. 10(b). The form of the strain energy release curves suggests that there is a driving force for a flaw located with one end a distance from the corner to extend into the corner and then through the oxide on the side to the free surface. The longer the flaw, the greater is the strain energy release rate for this extension with the energy being provided by the release of constraint on the expansion of the oxide from its compressed state attached to the alloy. Nevertheless, depending on the interface fracture resistance, there will still exist a critical length of flaw below which the flaw cannot extend because the available strain energy release rate is insufficient to exceed the fracture resistance of the interface. An interesting feature of the fracture energetics is that the strain energy release rate of the end of the crack, B, further from the corner is small and relatively independent of the crack size so there is very little driving force for the crack to extend *away* from the corner as distinct to towards the corner.

The computations, suggesting that a critical sized interface flaw near the corner can extend to the corner and then through the side oxide, prompts a comparison with the propagation of an edge flaw, C, in the side oxide in the same plane as the top oxide/alloy interface (Fig. 8(c)). The computed strain energy release rate is shown in Fig. 11 by the curves labeled D. The strain energy release rate is initially zero since it is propagating into a film under residual compression but rapidly increases in magnitude as the oxide/metal interface is approached. The abrupt change in sign of the local stresses due to the stress singularity at the corner makes it difficult to compute the value at the interface but thereafter the strain energy release slowly falls and approaches the steady-state value given by G_{SS} at distances of tens of oxide thickness. For further comparison, the strain energy release rates for a crack nucleating at the edge of a biaxially stressed film on a thick substrate are also shown, one for the film under tension and the other for the film under compression. (The solution for the crack at the edge of a compressed film has previously been computed as has the solution for a film under tension [15]). These two curves are almost the same and they too approach the steady-state value slowly over distances of tens of oxide thicknesses. For the film under compression, the crack is closed and the crack surfaces were treated as contacting surfaces in the finite element calculations. Comparison of the strain energy release rates shown in Figs. 10 and 11 suggest that edge cracking into the oxide is unlikely and that more favorable is the

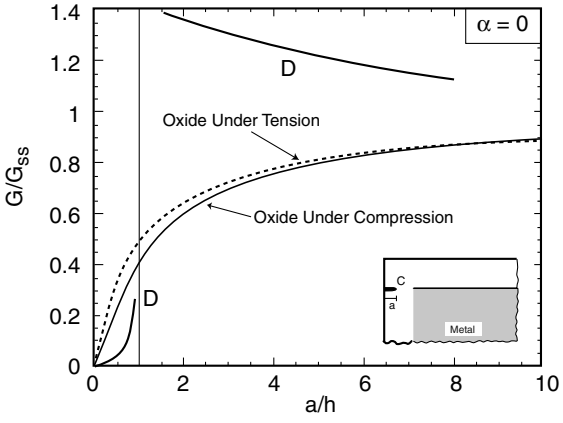

Fig. 11. The strain energy release rate, D, for a crack at the surface of the oxide film lying in the plane of the top oxide/alloy interface. For comparison, the strain energy release rates are shown for an edge crack in a pre-stressed film, either in compression or tension.

propagation of an interface flaw into the corner and then through the oxide to the free surface.

The calculations just described are for the propagation of a flaw along the oxide/alloy interface on one side of the step only. However, as the stress state is symmetrical about the step edge it is possible, in principle, for a flaw to propagate simultaneously from the corner along both the side and top of the step, as shown schematically in Fig. 8(d). As this would increase the overall displacement of the oxide from the alloy, one might expect that the strain energy released would also be larger than where the flaw extends along only one interface. This is borne out by finite element computations. Fig. 12 presents the strain energy release rate and phase angle for this symmetrical crack extension. One curve is for the oxide and the alloy having the same elastic constants and the other with the elastic modulus of the oxide being twice that of the alloy. As in other examples of residual stress fields, the strain energy release rate increases from zero at zero crack length to a maximum value and then decreases. The striking feature

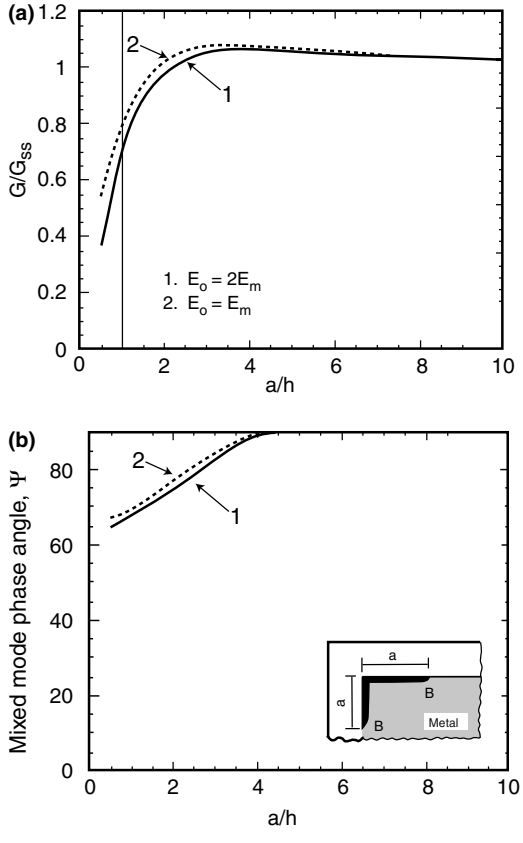

Fig. 12. Strain energy release rate (a) and mode mixity phase angle (b) for the simultaneous extension of a crack along both sides of the corner. The dashed curve is for the case where the oxide and alloy have the same elastic constants. The solid curve is for the oxide having twice the elastic modulus as the alloy but with a Poisson ratio of the oxide adjusted so that the Dundurs parameter, β, is zero. Poisson ratio of the alloy assumed to be 0.35.

though is that the maximum occurs within only 3–4 times the oxide thickness and then barely decreases to the steady-state value of G_{SS}. Not only is the strain energy release rate considerably larger than for the crack end B extending along only one of the edge surfaces, shown in Figs. 9 and 10, but it also reaches a steady-state value rather than decreasing with crack extension as for the single crack. In addition, the mode of loading becomes pure mode II within a very short distance (~4–5 times the oxide film thickness) of the corner, again in contrast to the case of the extension along a single side of the edge (Figs. 9 and 10). As the strain energy release rate is almost independent of crack length and propagates under mode II conditions away from the corner itself, the crack will be susceptible to kinking out of the interface plane to cause spalling. The distance from the corner at which the crack will kink out of the interface will depend on the location of flaws in the oxide and so one might expect considerable variability in the length of the spalled oxide on the grain surfaces. The statistical distribution of flaws in the oxide is believed to account for the variation in the length of the spalled oxide, as shown in Figs. 1, 2 and 6.

In summary, the strain energy release rate for cracking from a step edge is most likely to exceed the interface fracture resistance for those cases where flaws propagate simultaneously along both sides of the step. This is consistent with the majority of our observations, such as that in Figs. 1 and 6, where the oxide has spalled away along both the top and the sides of the uplifted grains. However, further investigation, in particular of the stability of a crack extending along two interfaces simultaneously, as well as the conditions under which they can kink-out of the interfaces, needs to be carried out since this is an area of fracture mechanics that has not been studied thoroughly. Such studies would also include detailed computations of the effect of various geometric factors including the angle of the step and the step height.

5. Discussion and implications

Underlying the phenomena described in this contribution is the ability of the evolving stresses in a growing oxide film to cause shape changes in plastically deformable alloy substrates. Early studies of the oxidation of metals demonstrated that thin sheets elongate, helical wires grow and hollow tubes extended upon oxidation if their sections were sufficiently thin [16]. More recently, the compressive growth stress in thermally grown oxides has been shown to motivate the "wrinkling" of a flat oxide on isothermal oxidation [17] and contribute to the "rumpling" of Pt modified NiAl oxidation coatings on cyclic oxidation [18]. These last two shape change phenomena can, in turn, promote failure of the oxide, and

over-coats, such as thermal barrier coatings, on cooling to ambient. Now to this catalog can be added the findings described in this work: if the alloy deforms by grain sliding in response to the growth stress, the shape changes at the edges of uplifted grains can create stress singularities that can, in turn, cause failure of the protective oxide on cooling. This is of significance from a design perspective, since the singularities are created on what was an initially flat surface. Consequently, where thin alloy sections are susceptible to oxidation, the possibility of deformation by grain sliding must be assessed.

One of the notable features of the high-temperature oxidation of alumina-forming alloys is just how large the stresses can be. Because of the large thermal expansion mismatch between alumina and the alumina-forming metals, the thermoelastic stresses on cooling can be very large; values in the range 4–7 GPa, depending on the alloy, have been measured [19]. Superimposed on these large thermoelastic stresses are the growth stresses in the aluminum oxide itself that can also be large. For instance, values of the reported growth stresses range from ~0.5 GPa (for NiAl alloys) [20,21] to peak values of ~1.5 GPa for the FeCrAlY alloys [2]. Using these values for the stress in the oxide in the force balance equation (Eq. (1)), it can be appreciated that they can motivate plastic deformation at high temperatures in relatively large alloy sections as well as generate large strain energy release rates on cooling. The form of plastic deformation response at the oxidation temperature depends on the constitutive behavior of the alloy. Thus, even though the stresses involved can be very large, the sort of edge spalling observed can only occur when plastic deformation of the alloy is largely by grain boundary sliding. The observations reported here suggest that Kanthal A1 and the FeCrAlY alloys, both solution-hardened, deform by grain boundary sliding. In contrast, no sliding was observed when the MA 956 alloy was oxidized under the same conditions and no oxide spalling was observed either. The difference is attributed to the fact that MA 956 is a dispersion strengthened FeCrAl alloy and that grain boundary sliding is suppressed by dispersoids along its boundaries.

Finally, an analogous situation to that discussed in this contribution occurs at the corners of macroscopic shapes, for instance, at the corners of a square or rectangular sectioned alloy, after prolonged oxidation. The growth stresses in the oxide cause plastic flow in the corner region of the alloy and, over time, an initially right-angled corner deforms and becomes progressively more acute. If the oxide can continually deform to accommodate this change, it remains intact and attached to the deforming metal. Otherwise, for instance, on cooling, it cracks along the edge as shown in several figures in the literature, for instance, Fig. 4 in [22], or voids form beneath the oxide. If, however, the thermally grown oxide is covered with a non-compliant coating, for instance, a thermal barrier coating, then the coating itself may crack. One such example is shown in Fig. 6 of [21].

Acknowledgements

This work was supported by the Office of Naval Research through Grant N00014-97-1-0190. The authors are grateful to A.G. Evans for the helpful discussions on crack kinking and to the reviewer for several helpful suggestions.

References

[1] Tolpygo VK, Dryden JR, Clarke DR. Acta Mater 1998;46:927.
[2] Tolpygo VK, Clarke DR. Oxid Metals 1998;49:187.
[3] Lipkin DM, Clarke DR. Oxid Metals 1996;45:267.
[4] Mennicke C, Ruhle M, Clarke DR. Oxid Metals 2001;55:551.
[5] Rhines FN, Wolf JS. Met Trans 1970;1:1701.
[6] Clarke DR. Acta Mater 2003;51:1393.
[7] Kanthal Corporation, Sweden.
[8] Tolpygo VK, Clarke DR. Mater Sci Engng A 2000;278:142.
[9] Tolpygo VK, Clarke DR. Mater Sci Engng A 2000;278:151.
[10] Hutchinson JW, Suo Z. Adv Appl Mech 1992;29:63.
[11] He MY, Bartlett A, Evans AG, Hutchinson JW. J Am Ceram Soc 1991;74:767.
[12] Timoshenko SP, Goodier JN. Theory of elasticity. 3rd ed.
[13] Yu HH, He MY, Hutchinson JW. Acta Mater 2001;49:93.
[14] Evans H. Int Metal Rev 1995;40:1.
[15] Suo Z. J Mech Phys Solids 1995;43:829.
[16] Tolpygo VK, Clarke DR. Acta Mater 2000;48:3283.
[17] Lipkin DM, Clarke DR. Oxid Metals 1996;45:267.
[18] Lipkin DM, Clarke DR, Hollatz M, Bobeth M, Pompe W. Corros Sci 1997;39:231.
[19] Sarioglu C, Schumann E, Blanchere JR, Petit FS, Meier GH. In: Newcomb SB, Little JA, editors. Microscopy of oxidation 4. London: Institute of Materials; 2000. p. 109.
[20] Engell H, Wever F. Acta Mater 1957;5:695.
[21] Tolpygo VK, Clarke DR. In: Dahotre NB, Hampikian JM, Morral JE, editors. Elevated temperature coatings: IV. TMS; 2001. p. 94.
[22] Engell H, Wever F. Acta Met 1957;5:695.